Original Article

Institution of MECHANICAL ENGINEERS

Journal of ENGINEERING TRIBOLOGY

Proc IMechE Part J:
J Engineering Tribology
0(0) 1–14

DOI: 10.1177/1350650117691697
journals.sagepub.com/home/pij
SAGE

Linear stability analysis of finite length journal bearings in laminar and turbulent regimes

Mohammad Miraskari[1], Farzad Hemmati[1], MY Alqaradawi[2] and Mohamed S Gadala[1,3]

Abstract

Dynamic coefficients of a finite length journal bearing are numerically calculated under laminar and turbulent regimes based on Ng–Pan–Elrod and Constantinescu models. Linear stability charts of a flexible rotor supported on laminar and turbulent journal bearings are found by calculating the threshold speed of instability associated to the start of instable oil whirl phenomenon. Local journal trajectories of the rotor-bearing system were found at different operating conditions solely based on the calculated dynamic coefficients in laminar and turbulent flow. Results show no difference between laminar and turbulent models at low loading while significant change of the size of the stable region was observed by increasing the Reynolds number in turbulent models. Stable margins based on the laminar flow at relatively low Sommerfeld numbers $S \leqslant 0.05$ were shown to fall inside the unstable region and hence rendering the laminar stability curves obsolete at high Reynolds numbers. Ng-Pan turbulent model was found to be generally more conservative and hence is recommended for rotor-bearing design.

Keywords

Finite length journal bearing, dynamic coefficients, stability, oil whirl, threshold speed of instability, Ng–Pan–Elrod and Constantinescu turbulent models

Date received: 22 June 2016; accepted: 29 December 2016

Introduction and literature survey

The ever increasing demand for injecting natural gas underground at high pressures was the incentive for the design of multistage compressors. One common fault in such compressors had been excessive lateral vibrations that were identified as sub-synchronous whirl.[1] Ideally a rotor is designed just to undergo the spin mode of motion. However, rotors undergo a different preceding type of motion known as rotor whirling that can be caused by a variety of mechanisms such as imbalance and misalignment with whirl frequencies of equal (synchronous) and higher (super-synchronous) than the spin speed of the shaft, respectively. In turbomachinery, an instability is usually referred to rotor whirling at frequencies other than the rotating spin frequency of the shaft.

Although sub-synchronous rotor whirling is not the most common type of instability, when it does occur at certain operating conditions, it can lead to high amplitude and potentially destructive lateral vibrations in the system. The necessary condition for occurrence of such whirling modes is when the operating spin speed of the shaft exceeds a threshold speed known as "threshold speed of instability" causing sub-synchronous whirling known as oil whirl/whip.[2] Linearized stiffness and damping coefficients are frequently used as the basis for stability analysis of the rotor-bearing systems in an aim to find the threshold speed of instability of a rotor-bearing system. The linearized coefficients are evaluated at the equilibrium position of the journal and are commonly calculated either by the infinitesimal approach of Lund[3] or the finite perturbation approach similar as in Qiu and Tieu.[4]

The Journal bearing force is a strong nonlinear function of its position with respect to the bearing chamber. However, the stability of the rotor-bearing

[1]Mechanical Engineering Department, University of British Columbia, Vancouver, Canada
[2]Department of Mechanical & Industrial Engineering, College of Engineering, Qatar University, Doha, Qatar
[3]Mechanical Engineering Department, Abu Dhabi University, Abu Dhabi, UAE

Corresponding author:
Mohammad Miraskari, Mechanical Engineering Department, University of British, Vancouver 2054-6250, BC, Canada.
Email: m.miraskari@alumni.ubc.ca

system can be characterized by means of linear analysis with the use of linearized bearing dynamic coefficients. It is known that the "local" stability of a non-linear system is essentially the same as the local stability of its linearized form, even though their stability type and global stability could be different. Local stability analysis is valid, only if the operating condition of interest is close enough to an operating equilibrium point or a fixed point of the system. Being close to a fixed point of the system is also a requirement for accurately estimating the linearized dynamic coefficients of the system, although there are different reports on the minimum required distance from fixed points to obtain accurate results. Lund[3] used the infinitesimal approach for obtaining the dynamical coefficients where the induced bearing pressure is perturbed by an infinitesimal amount through perturbing the oil film thickness. The operating points arising from infinitesimal perturbation of the system are by definition very close to the steady-state points of the system. He reported that the obtained coefficients are valid up to 40% of the bearing clearance. As an alternative approach for obtaining the dynamic coefficients, finite perturbations of the journal position and velocity are carried out combined with direct numerical differencing to obtain the linearized coefficients. Qiu and Tieu[4] studied the effect of perturbation amplitudes and concluded that the finite perturbation-based calculated coefficients are within 2.5% of those obtained by the infinitesimal approach if the perturbations of displacement and velocity are kept less than 5% and 4%, respectively. Choy et al.[5] calculated nonlinear bearing stiffness coefficients and showed that oil film forces will exhibit nonlinearities when displacements are sufficiently far from the steady-state operating point. San-Andres and Santiago[6] obtained the dynamic coefficients under high dynamic loads for which the journal moved in large orbital motions of up to 50% of the bearing clearance and found good agreement with analytical linearized coefficients. Meruane and Pascual[7] calculated linear and nonlinear bearing coefficients under large orbital motion and showed that the linearized analytical coefficients agree reasonably with numerically obtained linear coefficients. They reported negligible variations between the linear and nonlinear models provided that the operating speed is kept below the instability threshold speed. Weimin et al.[8] and Yang et al.[9] used an infinitesimal approach to calculate the linear and nonlinear bearing coefficients. Their results indicate close similarity between linear and nonlinear coefficients for eccentricity ratios of up to $\epsilon = 0.8$. They reported that linearized results will be incorrect at very high journal loads, especially for $\epsilon > 0.95$.

The majority of the stability studies of rotor-bearing systems in the literature are based on the declaration that fluid-film flow remains laminar throughout the operation of the machine. For large and heavy load bearings that run at high spin speeds and utilize low kinematic viscosity lubricants, the oil film flow becomes turbulent. To correctly identify the instability phenomenon and the oil whirl threshold speed of instability, the flow regime (whether laminar or turbulent) needs to be taken into account. This requires including the turbulent effects on the dynamic fluid forces as predicted by the Reynolds lubrication equation. Hashimoto and Wada[10,11] and Wang and Khonsari[12] investigated turbulent journal bearing performance under dynamic conditions for short bearings. They linearized turbulent coefficients in the Ng–Pan–Elrod model in an attempt to derive analytical expressions for journal force. However, their implemented linearization can lead to erroneous force predictions at large eccentricity ratios and high Reynolds numbers. Chang-Jian and Chen[13,14] investigated the dynamics of a flexible rotor bearing system supported by two turbulent journal bearings. They neglected the spatial gradients of turbulent coefficients to simplify the pressure and force calculations to obtain closed-form solutions. Their simplifying assumption can also lead into erroneous performance predictions.

In this paper, the pressure distributions of turbulent finite length journals are obtained by proper numerical solutions to modify Reynolds lubrication equation. Two turbulent models of Ng–Pan and Elrod and Constantinescu were implemented in the modified equation for comparison purposes. The calculated pressures are then used as the basis of the infinitesimal perturbation method in finding the turbulent dynamic coefficients for a range of operating conditions. Having the dynamic coefficients, the threshold speed of instability of a flexible shaft supported on end laminar and turbulent journals is found by means of linear stability analysis. Stability bounds are then compared for different shaft stiffness and Reynolds numbers ranging from laminar to fully turbulent flows in an attempt to study the range of applicability of original Reynolds equation and to find the operating conditions for which the modified analysis under turbulent conditions is necessary for obtaining accurate stability bounds. The journal bearing trajectories are also obtained by means of fast and robust implicit integration techniques for laminar and turbulent regimes solely based on the calculated dynamic coefficients.

Governing equations

Figure 1(a) shows a schematic of a journal bearing inside the bearing clearance. A simple rotor-bearing system can be represented as a concentrated mass supported on journal bearings modeled as direct and cross-coupled spring and dampers as shown in Figure 1(b) (cross coupling not shown).

Under static equilibrium, the weight of the rotor and journal is in balance with the bearing force such

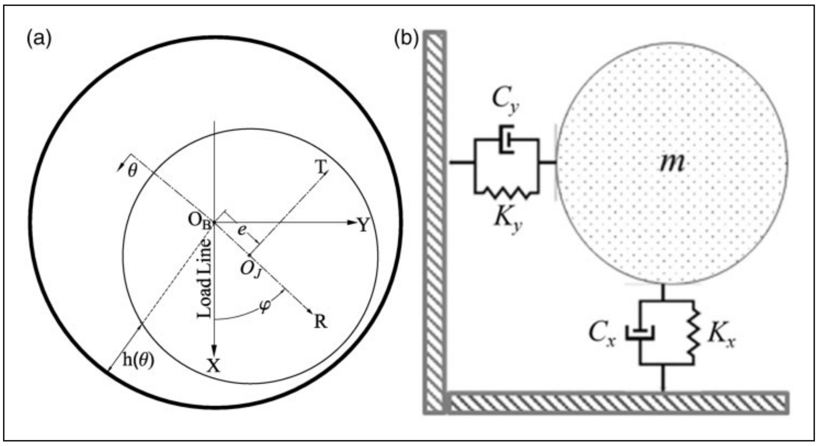

Figure 1. The schematic of a journal inside bearing (a) and modeling the effect of journal bearings with linear stiffness and damping coefficients (b).

that $\vec{F}+\vec{W}=0$ and hence relative to the static equilibrium state, the x and y components of the dynamic deviation of bearing force upon the rotor can be expressed as follows

$$\begin{aligned} F_x + W_x = f_x = \frac{\partial F_x}{\partial x}dx + \frac{\partial F_x}{\partial \dot{x}}\mathrm{d}\dot{x} + \frac{\partial F_x}{\partial y}dy \\ + \frac{\partial F_x}{\partial \dot{y}}\mathrm{d}\dot{y} + (higher\ order\ terms) \\ F_y + W_y = f_y = \frac{\partial F_y}{\partial x}dx + \frac{\partial F_y}{\partial \dot{x}}\mathrm{d}\dot{x} + \frac{\partial F_y}{\partial y}dy \\ + \frac{\partial F_y}{\partial \dot{y}}\mathrm{d}\dot{y} + (higher\ order\ terms) \end{aligned} \tag{1}$$

It is convenient to write equation (1) in the following matrix form

$$\begin{Bmatrix} f_x \\ f_y \end{Bmatrix} = -\begin{bmatrix} K_{xx} & K_{xy} \\ K_{yx} & K_{yy} \end{bmatrix}\begin{Bmatrix} x \\ y \end{Bmatrix} - \begin{bmatrix} C_{xx} & C_{xy} \\ C_{yx} & C_{yy} \end{bmatrix}\begin{Bmatrix} \dot{x} \\ \dot{y} \end{Bmatrix} \tag{2}$$

where $K_{ij} \equiv -\left(\partial F_i/\partial x_j\right)$ and $C_{ij} \equiv -\left(\partial F_i/\partial \dot{x}_j\right)$ are the eight bearing stiffness and damping coefficients as proposed by Lund.[15] The bearing reaction force can be calculated by integrating the oil-induced pressure over the surface of the journal

$$\begin{aligned} F_R = \int_0^{\theta_{cav}} R\mathrm{d}\theta \int_{-\frac{L}{2}}^{\frac{L}{2}} P\cos(\theta)\mathrm{d}z, \\ F_T = \int_0^{\theta_{cav}} R\mathrm{d}\theta \int_{-\frac{L}{2}}^{\frac{L}{2}} P\sin(\theta)\mathrm{d}z \end{aligned} \tag{3}$$

In order to calculate the oil induced pressure, one needs to solve the Reynolds partial differential equation for laminar flow

$$\frac{1}{R^2}\frac{\partial}{\partial \theta}\left(\frac{h^3}{12\,\mu}\frac{\partial P}{\partial \theta}\right) + \frac{\partial}{\partial z}\left(\frac{h^3}{12\,\mu}\frac{\partial P}{\partial z}\right) = \frac{1}{2}\omega\frac{\partial h}{\partial \theta} + \frac{\partial h}{\partial t} \tag{4}$$

Table 1. Turbulent constants of Constantinescu and Ng–Pan–Elrod model.

	Turbulence methods	
Constants	Constantinescu Model	Ng–Pan–Elrod Model
a_1	0.0198	0.0044
a_2	0.741	0.96
a_3	0.026	0.0136
a_4	0.8265	0.9

In relatively large diameter ($d > 0.4m$) journal bearings, the flow state becomes turbulent at low rotating speeds ($\omega < 400\ rpm$), when using low-viscosity lubricants, or when operating with large clearances. The state of the flow in fluid-film journal bearings can be judged by its Reynolds number. Turbulence comes into an effect at Reynolds number of approximately 2000 and higher.[16] For unsteady, incompressible turbulent flows in the oil film journal bearings as shown in Figure 1, the Reynolds equation can be written as

$$\frac{1}{R^2}\frac{\partial}{\partial \theta}\left(\frac{h^3}{k_\theta \mu}\frac{\partial P}{\partial \theta}\right) + \frac{\partial}{\partial z}\left(\frac{h^3}{k_z \mu}\frac{\partial P}{\partial z}\right) = \frac{\omega}{2}\frac{\partial h}{\partial \theta} + \frac{\partial h}{\partial t} \tag{5}$$

where k_θ and k_z are the turbulence coefficients in circumferential and longitudinal directions, respectively. In this paper, two turbulence methods are employed. First is the Constantinescu's model based on the Prandtl mixing length hypothesis,[17,18] and second is the Ng–Pan–Elrod model based on eddy viscosity.[17,19] The turbulence coefficients along with their constants for both employed models are presented in equation (6) and Table 1

$$\begin{cases} k_z = 12 + a_1(Re^*)^{a_2} \\ k_\theta = 12 + a_3(Re^*)^{a_4} \end{cases} \tag{6}$$

where Re^* is the local Reynolds number which varies with θ.

From equations (5) and (6), the turbulent Reynolds equation can be written as

$$\frac{1}{R^2}\frac{\partial}{\partial\theta}\left(\frac{h^3}{k_\theta\mu}\frac{\partial P}{\partial\theta}\right)+\frac{\partial}{\partial z}\left(\frac{h^3}{k_z\mu}\frac{\partial P}{\partial z}\right) = -\frac{C\epsilon\omega}{2}\sin(\theta)+C\dot{\epsilon}\cos(\theta)+C\epsilon\dot{\varphi}\sin(\theta) \tag{7}$$

If only the second term in the LHS of equation (4) is kept, an approximation which is within the acceptable range only for journal to length ratios of $\frac{L}{D}\leqslant 0.5$, solving the resulting ODE will yield the pressure in turbulent short bearings. It can be easily shown that the resulting pressure can be written as

$$P_{short}=\frac{k_z\mu}{h^3}\left[-\frac{C\varepsilon\omega}{2}\sin(\theta)+C\dot{\varepsilon}\cos(\theta)+C\varepsilon\dot{\emptyset}\sin(\theta)\right]\times\left(\frac{z^2}{2}-\frac{L^2}{8}\right) \tag{8}$$

Identification of bearing dynamic coefficients

Direct solution to equation (4) for laminar flow will yield the corresponding laminar pressure field. In order to obtain the journal bearing dynamic coefficients, the force derivatives with respect to displacement and velocity of the journal center are to be obtained such that $k_{ij}\equiv-\left(\partial F_i/\partial x_j\right)$ and $c_{ij}\equiv-(\partial F_i/\partial\dot{x}_j)$. The coefficients can now be directly calculated by first exerting some external finite perturbation at each steady-state point following direct numerical differentiation.[4,20,21] While finite perturbation approach may be adequate for practical purposes, the inherent numerical inaccuracy of the method can be eliminated by employing a perturbation solution known as the infinitesimal perturbation approach.[3] It is reported that provided the perturbation amplitudes are kept less than *0.02C* (displacement) or *0.02ωC* (velocity) for normal bearing eccentricities, the calculated dynamic coefficients will be within 0.1% of the infinitesimal approach.[4] An infinitesimal perturbation method is used in this work. Following references,[3,22] the lubricant thickness in steady state h_0 is perturbed in R and T directions (as in Figure 1(a)) in the form

$$\begin{aligned} h &= h_0+dh=h_0+dR\cos\theta+dT\sin\theta \\ \frac{\partial h}{\partial t} &= d\dot{R}\cos\theta+d\dot{T}\sin\theta \end{aligned} \tag{9}$$

This perturbation in film thickness will result to a perturbation of the pressure film as

$$P=P_0+dP=P_0+\frac{\partial P}{\partial R}dR+\frac{\partial P}{\partial T}dT+\frac{\partial P}{\partial\dot{R}}d\dot{R}+\frac{\partial P}{\partial\dot{T}}d\dot{T} \tag{10}$$

Equations (9) and (10) are substituted back into modified Reynolds Equation for turbulent flow (5) and keeping only zeroth- and first-order terms will omit the time-dependent terms and will yield five steady pressure and pressure gradient equations

$$\frac{1}{R^2}\frac{\partial}{\partial\theta}\left(\frac{h_0^3}{k_\theta\mu}\frac{\partial P_0}{\partial\theta}\right)+\frac{\partial}{\partial z}\left(\frac{h_0^3}{k_z\mu}\frac{\partial P_0}{\partial z}\right)=\frac{\omega}{2}\frac{\partial h_0}{\partial\theta} \tag{11}$$

$$\begin{aligned} &\frac{1}{R^2}\frac{\partial}{\partial\theta}\left(\frac{h_0^3}{k_\theta\mu}\frac{\partial P_R}{\partial\theta}\right)+\frac{\partial}{\partial z}\left(\frac{h_0^3}{k_z\mu}\frac{\partial P_R}{\partial z}\right) \\ &=-\frac{\omega}{2}\sin\theta-\frac{1}{R^2}\frac{\partial}{\partial\theta}\left(\frac{3\,h_0^2}{k_\theta\mu}\cos\theta\frac{\partial P_0}{\partial\theta}\right) \\ &\quad-\frac{\partial}{\partial z}\left(\frac{3\,h_0^2}{k_\theta\mu}\cos\theta\frac{\partial P_0}{\partial z}\right) \end{aligned} \tag{12}$$

$$\begin{aligned} &\frac{1}{R^2}\frac{\partial}{\partial\theta}\left(\frac{h_0^3}{k_\theta\mu}\frac{\partial P_T}{\partial\theta}\right)+\frac{\partial}{\partial z}\left(\frac{h_0^3}{k_z\mu}\frac{\partial P_T}{\partial z}\right) \\ &=\frac{\omega}{2}\cos\theta-\frac{1}{R^2}\frac{\partial}{\partial\theta}\left(\frac{3\,h_0^2}{k_\theta\mu}\sin\theta\frac{\partial P_0}{\partial\theta}\right) \\ &\quad-\frac{\partial}{\partial z}\left(\frac{3\,h_0^2}{k_\theta\mu}\sin\theta\frac{\partial P_0}{\partial z}\right) \end{aligned} \tag{13}$$

$$\frac{1}{R^2}\frac{\partial}{\partial\theta}\left(\frac{h_0^3}{k_\theta\mu}\frac{\partial P_{\dot{R}}}{\partial\theta}\right)+\frac{\partial}{\partial z}\left(\frac{h_0^3}{k_z\mu}\frac{\partial P_{\dot{R}}}{\partial z}\right)=\cos\theta \tag{14}$$

$$\frac{1}{R^2}\frac{\partial}{\partial\theta}\left(\frac{h_0^3}{k_\theta\mu}\frac{\partial P_{\dot{T}}}{\partial\theta}\right)+\frac{\partial}{\partial z}\left(\frac{h_0^3}{k_z\mu}\frac{\partial P_{\dot{T}}}{\partial z}\right)=\sin\theta \tag{15}$$

A solution of the modified Reynolds differential equation for steady pressure (equation (11)) has been obtained numerically using finite volume method with successive over-relaxation scheme (point Gauss–Seidel with over relaxation parameter $\omega = 1.4$). A sample mesh of 100×30 (θ, z) was selected to calculate the pressure field for a low Reynolds number operating point at eccentricity ratio of $\epsilon = 0.8$. The calculated pressure is non-dimensionalized and is shown along with the mesh in Figure 2. The pressure boundary condition is the commonly used Swift–Stieber boundary condition for a fully cavitated journal bearing such that $P=\frac{\partial P}{\partial\theta}=0\ at\ \theta=\theta_{cav}$ for the cavity zone and zero pressure at the journal edges $P_0=dP=0\ at\ Z=\pm\frac{L}{2}$.[21]

The pressure distributions (non-dimensionalized) of the finite length journal for laminar and both available turbulent models are calculated at the journal mid-span and are compared to available analytical solutions of a short bearing in Figure 3. The corresponding pressure distributions are evaluated for two

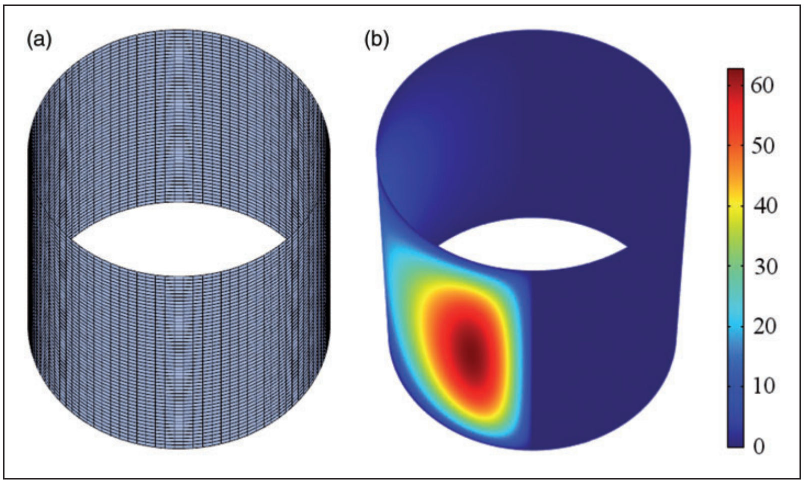

Figure 2. The selected mesh (a) and non-dimensional pressure distribution, $\bar{P}$, on the journal surface for a cavitated journal bearing (b).

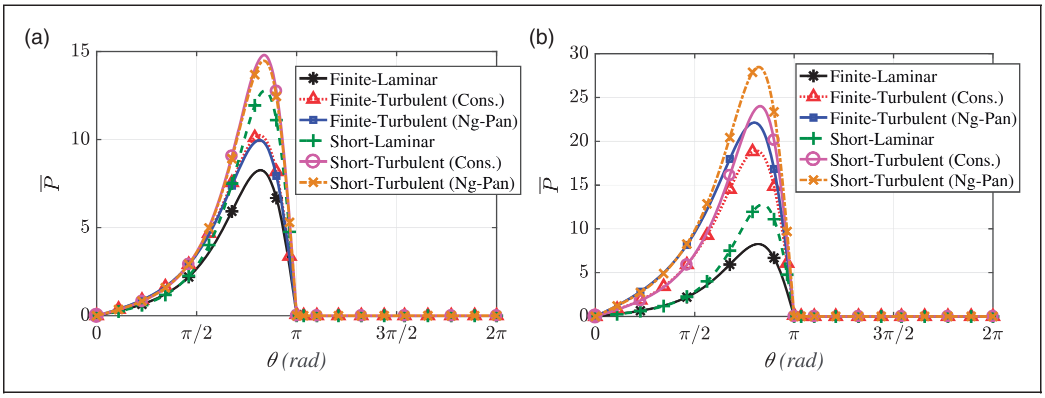

Figure 3. The comparison of numerically and analytically obtained pressure (non-dimensional) distributions at mid-span of a finite length journal bearing with $\frac{L}{D} = \frac{1}{2}$ for laminar and turbulent flow at $\varepsilon = 0.6$ and Re = 1000: (a) and Re = 10000 (b).

different cases at $\varepsilon = 0.6$. First, at a low Reynolds number of $Re = 1000$ (well into the laminar region) as shown in Figure 3(a) and then for a relatively high Reynolds number of $Re = 10000$ (fully turbulent) as shown in Figure 3(b). Results indicate that as the Reynolds number increases, the predicted pressure distributions of the modified Reynolds equation deviates increasingly from the pressures as predicted by classical Reynolds equation. The predicted pressures of a turbulent bearing for both turbulent models are sufficiently close at low Reynolds numbers but pressure predictions of Ng-Pan method becomes increasingly different from the pressure predictions based on the Constantinescu model at higher Reynolds numbers.

The obtained pressure field is then used as the basis for calculation of the pressure field gradients according to equations (12) to (15). Having all the pressure gradients calculated in the R-T coordinate system, the dynamic coefficients can be simply found by integrating the pressure gradients over the non-cavitated flow region[3] on the journal surface according to the Swift–Stieber boundary condition

$$\begin{aligned}
\begin{Bmatrix} K_{rr} \\ K_{tr} \end{Bmatrix} &= -\int_0^{\theta_{cav}} \int_{-\frac{L}{2}}^{\frac{L}{2}} P_R \begin{Bmatrix} \cos\theta \\ \sin\theta \end{Bmatrix} R\mathrm{d}\theta\mathrm{d}z, \\
\begin{Bmatrix} K_{rt} \\ K_{tt} \end{Bmatrix} &= -\int_0^{\theta_{cav}} \int_{-\frac{L}{2}}^{\frac{L}{2}} P_T \begin{Bmatrix} \cos\theta \\ \sin\theta \end{Bmatrix} R\mathrm{d}\theta\mathrm{d}z \\
\begin{Bmatrix} C_{rr} \\ C_{tr} \end{Bmatrix} &= -\int_0^{\theta_{cav}} \int_{-\frac{L}{2}}^{\frac{L}{2}} P_{\dot{R}} \begin{Bmatrix} \cos\theta \\ \sin\theta \end{Bmatrix} R\mathrm{d}\theta\mathrm{d}z, \\
\begin{Bmatrix} C_{rt} \\ C_{tt} \end{Bmatrix} &= -\int_0^{\theta_{cav}} \int_{-\frac{L}{2}}^{\frac{L}{2}} P_{\dot{T}} \begin{Bmatrix} \cos\theta \\ \sin\theta \end{Bmatrix} R\mathrm{d}\theta\mathrm{d}z
\end{aligned} \tag{16}$$

Having the dynamic coefficients matrices $\boldsymbol{k}$ and $\boldsymbol{c}$ in R–T coordinates, a simple coordinate transformation with angle of rotation being the attitude angle φ will yield the bearing coefficients in x–y coordinate system

$$Q = \begin{pmatrix} \cos\varphi & -\sin\varphi \\ \sin\varphi & \cos\varphi \end{pmatrix}, \quad [\bar{K}]_{x-y} = -Q[\bar{K}]_{R-T}\, Q^T, \quad [\bar{C}]_{x-y} = -Q[\bar{C}]_{R-T} Q^T \tag{17}$$

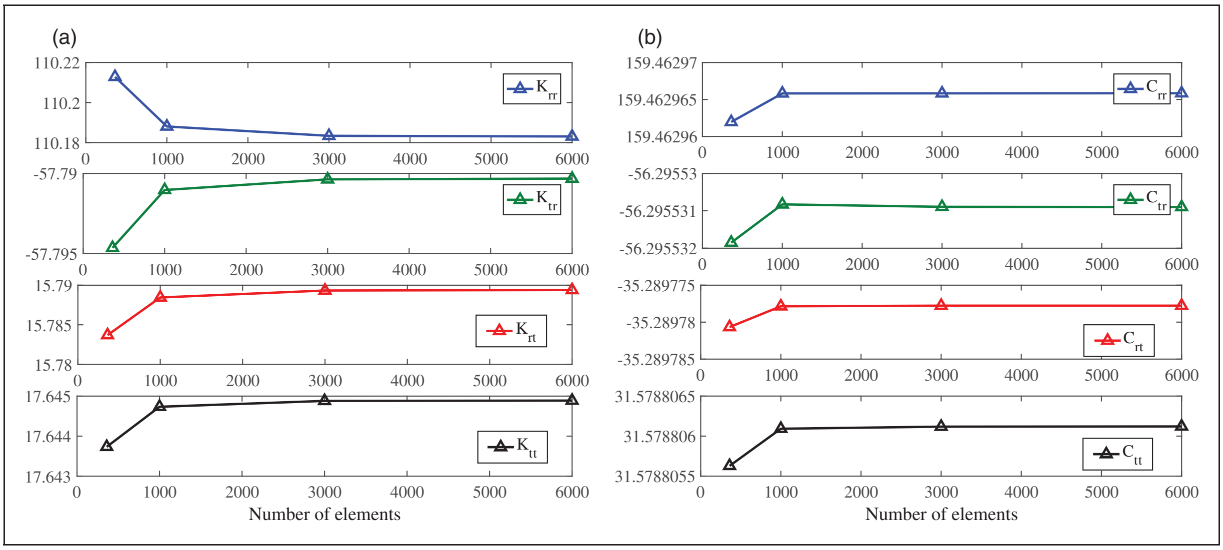

Figure 4. Non-dimensional stiffness (a) and damping (b) coefficients as target variables for mesh sensitivity analysis.

Table 2. Sample calculations of discretization errors.

	$\phi = P_{max}$	$\phi = K_{rr}$	$\phi = K_{tr}$	$\phi = K_{rt}$	$\phi = K_{tt}$
Φ_1 (fine grid)	61.6153	110.1834	−57.7904	15.7893	17.6449
Φ_2	61.4949	110.1880	−57.7910	15.7884	17.6447
Φ_3 (coarse grid)	61.5675	110.2128	−57.7946	15.7837	17.6437
Φ_{ext}^{21}	61.7984	110.1823	−57.7902	15.7895	17.6449
$\%e_a^{21}$	0.1953	4.24E-03	1.15E-03	5.55E-03	8.29E-04
$\%e_{ext}^{21}$	0.2963	9.83E-04	2.59E-04	1.26E-03	1.42E-04
$\%GCI_{fine}^{21}$	0.3715	1.23E-03	3.24E-04	1.57E-03	1.78E-04

Based on sensitivity analysis of the maximum pressure as a function of the number of divisions in the circumferential (θ) and axial (z) directions, it is reported in the literature that the solution is more sensitive to the circumferential mesh density.[7,23] A mesh density sensitivity analysis, similar to Miraskari et al.,[24] was carried out for four representative mesh sizes of 30×12, 50×20, 100×30 and $150 \times 40\,(\theta,\ z)$. The maximum field pressure as well as all stiffness and damping coefficients was selected as target variables (ϕ) of interest for mesh sensitivity analysis and are calculated at an eccentricity ratio of $\epsilon = 0.8$ for a finite length journal bearing with $\frac{L}{D} = 1$. Plots of stiffness and damping coefficients vs. total number of elements are shown in Figure 4.

The fine grid convergence index GCI_{fine}^{21} (an indicator of mesh numerical uncertainty) as well as extrapolated target variables and corresponding grid error for a subset of selected mesh (30×12, 50×20 and 100×30) was calculated based on Celik et al.[25] The fine grid convergence calculations for dynamic stiffness as target variables are tabulated in Table 2. The fine grid (100×30 $(\theta,\ z)$) convergence index GCI_{fine}^{21} indicating numerical uncertainty in calculating maximum target variable does not exceed 0.4% for maximum field pressure and does not exceed 0.0012% for any of the calculated dynamic coefficients and hence the final fluid model was selected with 100×30 $(\theta,\ z)$ divisions with a total of 3000 2D fluid elements.

The calculated values for stiffness and damping of a finite length journal bearing in laminar flow are compared to the analytically available coefficients of a short bearing for a length-to-diameter ratio $\frac{L}{D} = 1$ when plotted against the Sommerfeld number and are shown in Figure 5.

As can be seen from Figure 5, at high Sommerfeld numbers (lower static load on shaft and hence smaller eccentricity ratios), the numerically obtained coefficients from direct solution to the Reynolds equations will become increasingly closer to the analytically obtained short bearing values unlike the big deviations in the low Sommerfeld region (high load and or higher eccentricity ratios). This is of course expected because of the higher pressure relief of the short bearing compared to a finite length journal bearing especially at high static loads.

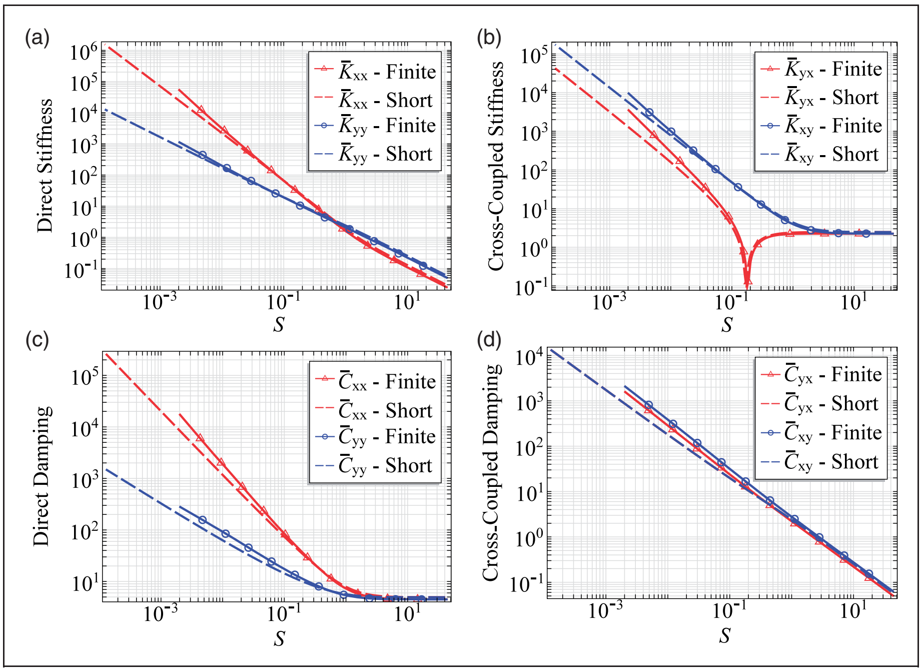

Figure 5. The comparison of numerically calculated laminar dynamic coefficients of a finite length journal bearing $\left(\frac{L}{D}=\frac{1}{2}\right)$ with analytical short bearing results. Direct stiffness (a), cross-coupled stiffness (b), direct damping (c), and cross-coupled damping (d).

Mathematical model of the rotor-bearing system

In an ideal and fully balanced rotor-bearing system, the shaft spins at its designed operating speed while the induced pressures inside end journals can support the weight of the shaft and hence there exists an equilibrium point where the journal center finds and stays there during the operation. This point is referred to as the static equilibrium position. If the rotor bearing system is undisturbed, the rotor will remain in its equilibrium position. For small disturbances, for instance small unbalance force, the shaft will no longer stay at the static equilibrium point and orbits via a closed elliptic curve around its equilibrium point. These are the harmonic solutions to a stable dynamic system operating in its stable region. If the operating speed of the shaft exceeds the so-called threshold speed of instability ω_{th}, no stable harmonic solution exists and the journal orbit will spiral outward towards an either bounded stable limit cycle (with orbits generally much greater than the stable closed harmonic orbits) or towards the point where metal to metal contact occurs. This change of the dynamical behavior of the system is called a bifurcation and is known in rotor dynamics terminology as the oil whirl–whip phenomenon. It should be noted that oil whirl and rotor whirling will happen for both fully balanced and unbalanced rotor with the exception that the threshold speed of a balanced system is higher than the threshold speed of an unbalanced system.

The transition (bifurcation) to high amplitude vibration, whether to a stable limit cycle or towards the bearing clearance, can be either gradual (supercritical bifurcation) or sudden (subcritical bifurcation). Bifurcation towards the limit cycle is generally considered as an unstable operating condition while it is not necessarily unstable. The reason for this is that the majority of the stability analysis available in the literature are based on linear analysis, and from the viewpoint of linear analysis there is no difference between unstable and stable limit cycles (they are both considered as unstable). Even though the bifurcation type cannot be evaluated via linear analysis, the stability margin can indeed be identified by simple linear analysis. This is because the local stability of nonlinear and linearized systems is essentially the same. Linearized analysis will be used here to identify the stability margins of the system. To do this, one needs to find the threshold speed of instability for a given rotor-bearing system at any applied static load to the shaft. If the operating speed of the rotor is kept below this threshold speed, the system remains in its stable region and hence the operation is considered as safe. The analysis here follows from literature.[21,26]

Referring to Figure 6, to analyze a flexible, center-loaded, and perfectly balanced rotor symmetrically supported by two identical fluid-film journal bearings, the following assumptions are made:

- Deflection of the flexible shaft is small to allow the use of linear beam theory.
- The mass of the shaft and rotor torque of the midpoint mass are negligible.
- The rotor mass is lumped at the midpoint.
- Axial and torsional vibrations of the lumped mass are negligible.

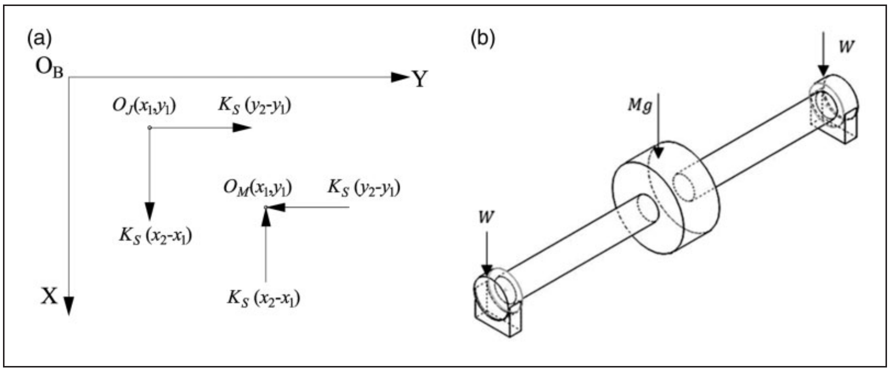

Figure 6. Schematic of a flexible rotor supported on journal bearings. O_J and O_M correspond to the geometric center of the journal and the central disc, respectively.

- Gyroscopic effect of the shaft, disk and journal bearings are negligible.

The equations of motion for the central disk and journal bearings may be written as follows

$$\mathit{Central\ Disk}:\begin{cases} M\,\ddot{x}_2 + K_s(x_2 - x_1) = 0 \\ M\,\ddot{y}_2 + K_s(y_2 - y_1) = 0 \end{cases},\qquad \mathit{Journal\ Bearings}:\begin{cases} -2dF_x + K_s(x_2 - x_1) = 0 \\ -2dF_y + K_s(y_2 - y_1) = 0 \end{cases} \tag{18}$$

where K_s is the shaft stiffness, and dF_x and dF_y are the components of the force due to induced bearing pressure in excess of the equilibrium forces and are calculated based on equation (2).

Assuming harmonic motion of the central disc and journals with frequency $\nu = Re(\nu) + i\,Im(\nu)$

$$\begin{pmatrix} x_1 \\ x_2 \end{pmatrix} = \begin{pmatrix} X_1 \\ X_2 \end{pmatrix} e^{\nu t},\quad \begin{pmatrix} y_1 \\ y_2 \end{pmatrix} = \begin{pmatrix} Y_1 \\ Y_2 \end{pmatrix} e^{\nu t} \tag{19}$$

By substituting equation (19) into equation (18), the following expression may be obtained

$$\begin{bmatrix} \left\{ \begin{matrix} \dfrac{-K_s M\nu^2}{K_s + M\nu^2} \\ +2K_{xx} + 2\nu C_{xx} \end{matrix} \right\} & 2K_{xy} + 2\nu C_{xy} \\ 2K_{yx} + 2\nu C_{yx} & \left\{ \begin{matrix} \dfrac{-K_s M\nu^2}{K_s + M\nu^2} \\ +2K_{yy} + 2\nu C_{yy} \end{matrix} \right\} \end{bmatrix} \times \begin{pmatrix} X_1 \\ X_2 \end{pmatrix} = \begin{pmatrix} 0 \\ 0 \end{pmatrix} \tag{20}$$

Non-dimensionalizing according to Szeri[21] for shaft and bearing stiffness and bearing damping and also having $\begin{pmatrix} \bar{X}_1 \\ \bar{X}_2 \end{pmatrix} = \frac{1}{C}\begin{pmatrix} X_1 \\ X_2 \end{pmatrix}$, $\omega = \bar{\omega}\sqrt{K_s/M}$, $\nu = \omega\bar{\nu}$, $\alpha = \frac{-\bar{K}_s\bar{\nu}^2\bar{\omega}^2}{1+\bar{\nu}^2\bar{\omega}^2}$, the non-dimensional from of equation (20) is

$$\begin{bmatrix} \alpha + 2\bar{K}_{xx} + 2\bar{\nu}\bar{C}_{xx} & 2\bar{K}_{xy} + 2\bar{\nu}\bar{C}_{xy} \\ 2\bar{K}_{yx} + 2\bar{\nu}\bar{C}_{yx} & \alpha + 2\bar{K}_{yy} + 2\bar{\nu}\bar{C}_{yy} \end{bmatrix} \begin{pmatrix} \bar{X}_1 \\ \bar{X}_2 \end{pmatrix} = \begin{pmatrix} 0 \\ 0 \end{pmatrix} \tag{21}$$

The condition of non-trivial (non-zero) solution requires that the determinant of the characteristic matrix needs to be set to zero. By setting the imaginary part of the determinant of equation (21) to zero

$$\alpha = \frac{2\left(\bar{K}_{xy}\bar{C}_{yx} + \bar{K}_{yx}\bar{C}_{xy} - \bar{K}_{yy}\bar{C}_{xx} - \bar{K}_{xx}\bar{C}_{yy}\right)}{\bar{C}_{xx} + \bar{C}_{yy}} \tag{22}$$

By setting the real part of the determinant of equation (21) to zero

$$\bar{\nu}^2 = \frac{\alpha^2 + 2\left(\bar{K}_{xx} + \bar{K}_{yy}\right)\alpha + 4\left(\bar{K}_{xx}\bar{K}_{yy} - \bar{K}_{xy}\bar{K}_{yx}\right)}{4\left(\bar{C}_{xy}\bar{C}_{yx} - \bar{C}_{xx}\bar{C}_{yy}\right)} \tag{23}$$

In the state of neutral stability, $\bar{\nu}$ is purely imaginary and $\frac{\nu_{whirl}}{\omega} = \sqrt{-\bar{\nu}^2}$. Having $\bar{K}_s = \frac{C}{L\,D\,\mu\,N\left(\frac{R}{C}\right)^2} K_s = \frac{1}{S}\frac{C\,K_s}{W}$ and using the definition of α, the instability threshold value can be found as

$$\bar{\omega}_{th}^2 = \frac{\alpha}{\bar{\nu}^2\left(\bar{K}_s - \alpha\right)} \tag{24}$$

Results and discussions

Laminar and turbulent dynamic coefficients

The finite length journal bearing pressure and pressure gradients in turbulent flow can be calculated by solving the steady and perturbed modified Reynolds equation, equations (11) to (15). The Coefficients in *R-T* coordinate system are then calculated by integrating the pressure gradients as in equation (16). A coordinate transformation as in equation (17) from R–T to X–Y is then necessary to find the coefficients in the X–Y coordinate system which is suitable for stability analysis. This is done for a range of Reynolds numbers (10,000, 20,000 and 30,000) and for both the Constantinescu and Ng–Pan–Elrod turbulent models and is compared to the calculated coefficients in the laminar region against the Sommerfeld number in Figure 7.

Similar treatment was carried out to calculate the damping coefficients of turbulent journal bearings. The calculated bearing damping coefficients in turbulent flow are compared to the previously calculated coefficients in the laminar region and are plotted against the corresponding Sommerfeld number in Figure 8.

By substituting the laminar and turbulent coefficients obtained based on the two different turbulent models (as was shown in Figures 7 and 8) into equations (22) to (24), one can obtain the stability margins of a flexible shaft supported by laminar and turbulent finite length journal bearings.

Identification of threshold speed of instability

The non-dimensional threshold speed of instability $\bar{\omega}_{th}$ is calculated to find the corresponding stability parameter $\gamma = \frac{C K_s}{W} \bar{\omega}_{th}^2$, for laminar and turbulent bearings at a range of Reynolds numbers. The stability parameter γ is plotted against the Sommerfeld number for different non-dimensional shaft stiffness parameter values as shown in Figure 9.

The expansion of stable region is observed for turbulent bearing supported shafts as shown in Figure 9. By comparing the stability of turbulent bearings to the laminar bearings and holding the non-dimensional shaft stiffness constant as in Figure 9(a) to (d), it is clear that the turbulent curves are shifted to the left of the laminar curve, indicating that the unstable region has grown in size. The added unstable region due to turbulent bearings is in the low Sommerfeld $S \leqslant 0.05$ (high loading) region. This suggests that as the static loading increases on the shaft, the turbulent bearings are progressively less stable compared to the bearing which is operating in the laminar region of oil film flow. At high Sommerfeld region $S \geqslant 0.2$ (low load), the stability curves of laminar and turbulent bearings are very much alike. This destabilizing effect of turbulent bearings increases by the Reynolds number. At each Reynolds and at each non-dimensional shaft stiffness, the stability curves of the Constantinescu's turbulent model are positioned above the curves obtained based on the Ng–Pan–Elrod turbulent model suggesting that the Ng–Pan–Elrod turbulent treatment is more

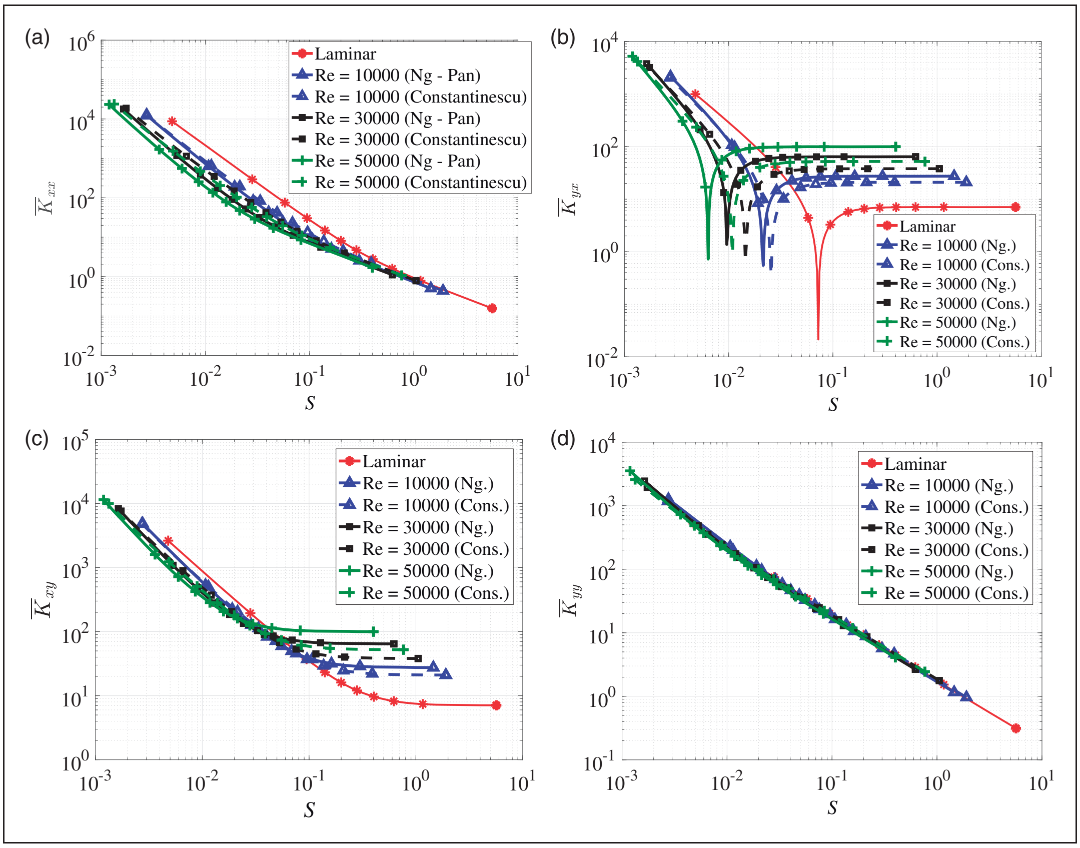

Figure 7. Comparison of the stiffness coefficients of a fully turbulent finite length journal bearing with the laminar (Reynolds independent) stiffness coefficients: $\bar{K}_{xx}$ (a), $\bar{K}_{yx}$ (b), $\bar{K}_{xy}$ (c), and $\bar{K}_{yy}$ (d).

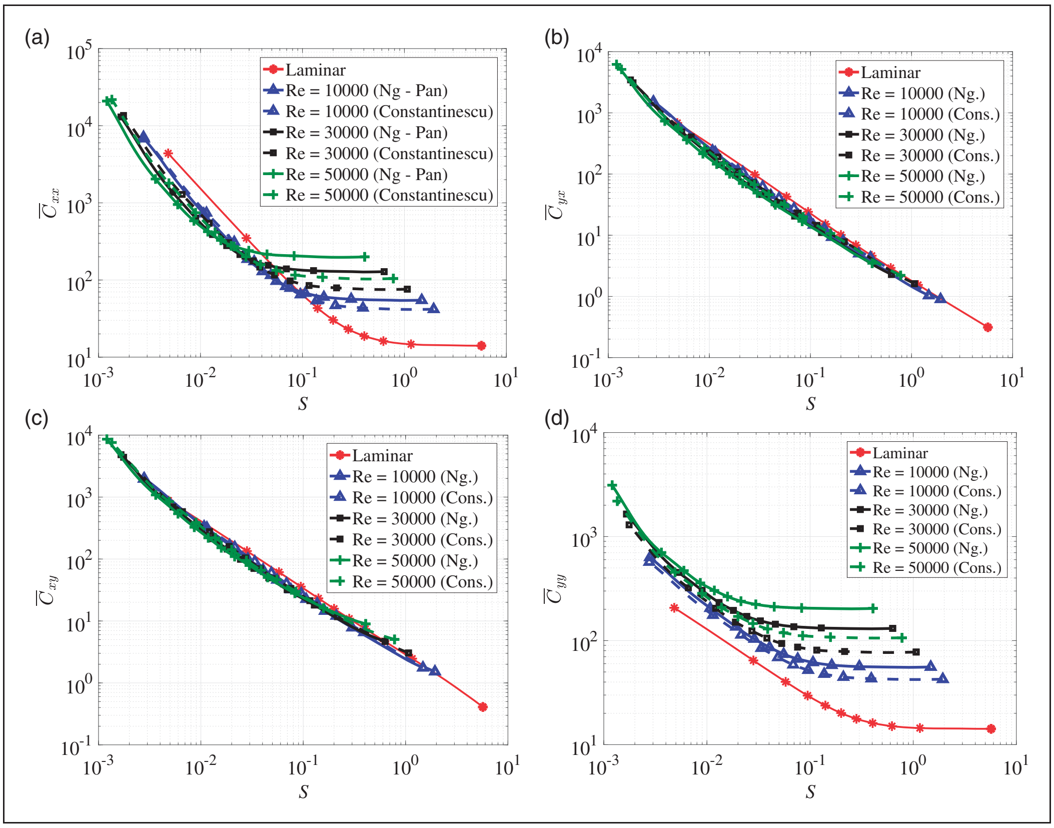

Figure 8. Comparison of the damping coefficients of a fully turbulent finite length journal bearing with the laminar (Reynolds independent) damping coefficients: $\bar{C}_{xx}$ (a), $\bar{C}_{yx}$ (b), $\bar{C}_{xy}$ (c), and $\bar{C}_{yy}$ (d).

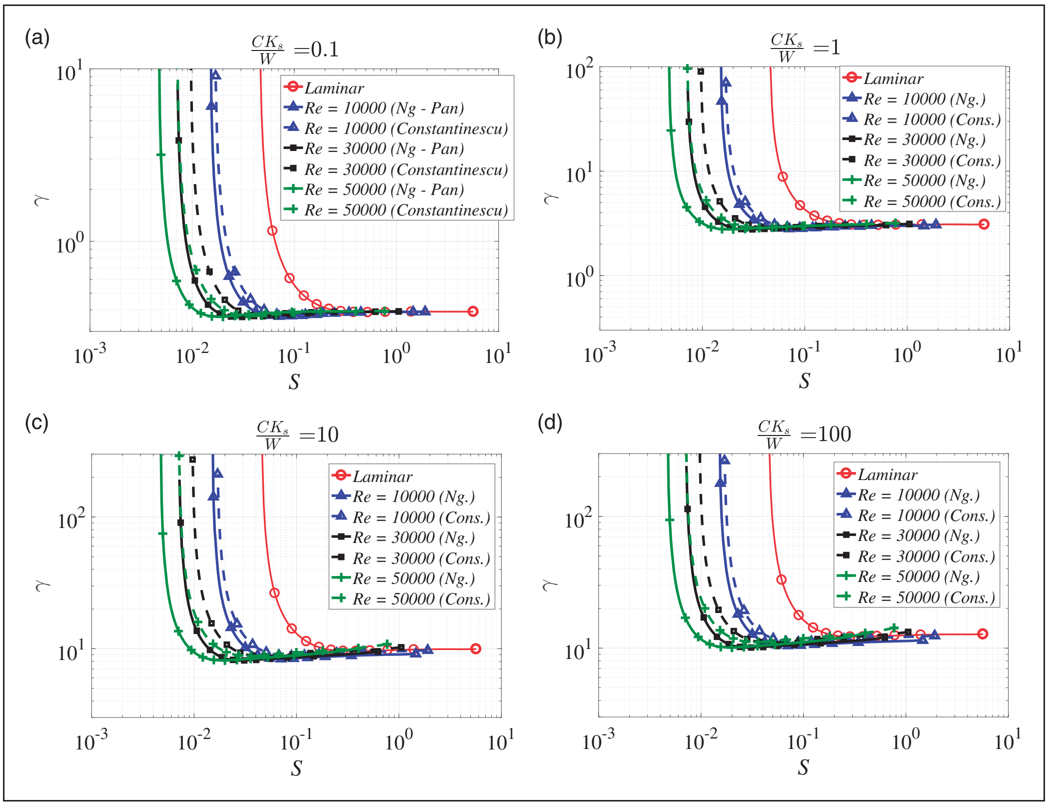

Figure 9. Linear stability curves of a flexible shaft supported on laminar and turbulent finite length journal bearings at ends against the Sommerfeld number for a range of non-dimensional shaft stiffness $\frac{CK_s}{W} = 0.1$ (a), $\frac{CK_s}{W} = 1$ (b), $\frac{CK_s}{W} = 10$ (c), and $\frac{CK_s}{W} = 100$ (d).

conservative when used as basis for design of the rotor-bearing system.

Rotor-bearing system trajectories

To illustrate the expansion of the unstable operating region and shortcoming of the laminar theory in predicting the stable regions of the rotor-bearing system, the journal trajectories at different operating points should be calculated. To do this, the set of governing equations of motion for the journal and the shaft are to be numerically calculated to obtain the trajectory of the journal center. This is done first by transforming the linear ODE system of equation (18) into state–space representation of the form $\dot{X} = f(X, t)$ as follows

$$
\begin{aligned}
\dot{X}_1 &= \frac{\left\{\begin{array}{c} C_{xy}(K_s X_2 - K_s X_4 + 2K_{yx}X_1 + 2K_{yy}X_2) \\ -C_{yy}(K_s X_1 - K_s X_3 + 2K_{xx}X_1 + 2K_{xy}X_2) \end{array}\right\}}{2C_{xx}C_{yy} - 2C_{xy}C_{yx}} \\
\dot{X}_2 &= \frac{\left\{\begin{array}{c} C_{yx}(K_s X_1 - K_s X_3 + 2K_{xx}X_1 + 2K_{xy}X_2) \\ -C_{xx}(K_s X_2 - K_s X_4 + 2K_{yx}X_1 + 2K_{yy}X_2) \end{array}\right\}}{2C_{xx}C_{yy} - 2C_{xy}C_{yx}} \\
\dot{X}_3 &= X_5 \\
\dot{X}_4 &= X_6 \\
\dot{X}_5 &= \frac{-K_s(X_3 - X_1)}{M} \\
\dot{X}_6 &= \frac{-K_s(X_4 - X_2)}{M}
\end{aligned}
\tag{25}
$$

where (X_1, X_2) and (X_3, X_4) are (x, y) position coordinates of the journal center and the mass disk center respectively. The journal bearing coefficients in equation (18) are time varying functions of the journal center (X_1, X_2). It shall be noted that trajectories can be solely obtained based on the linearized coefficients provided that the journal position remains close to its steady-state position. The system of equation (25) can be used as basis for calculation of the journal trajectories for much more complicated systems provided that the dynamic coefficients are available (either previously calculated or experimentally obtained).

The system of coupled linear ODEs of equation (25) is integrated numerically by an implicit scheme to obtain the trajectories of the journal and the disk center. When the journal force is expressed in terms of dynamic coefficients, the Jacobian of the linear ODE system can be easily calculated and hence can be used effectively in an implicit time integration scheme. A first-order Implicit Euler method is adopted here

$$\dot{X} = \frac{X^{n+1} - X^n}{\delta t} = \frac{\delta X}{\delta t} = f^{n+1}(X, t) \tag{26}$$

where superscripts n and $n+1$ represent a variable value at the current and the next time-step, respectively. The next step is to express the right hand side of equation (26), $f^{n+1}(X, t)$, in terms of the functions of the variable and its gradients at the current time-step through a Taylor series expansion

$$f^{n+1}(X, t) = f\left(X^{n+1}\right) = f(X^n + \delta X) = f(X^n) + \left.\frac{\partial f}{\partial X}\right|^n \delta X + H.O.T \tag{27}$$

where $\left.\frac{\partial f}{\partial X}\right|^n$ is the Jacobian matrix of the linear ODE system evaluated at the current time-step and takes the following form

$$
J(X) = \frac{\partial f}{\partial X} = \begin{pmatrix}
\frac{C_{yy}K_s + 2C_{yy}K_{xx} - 2C_{xy}K_{yx}}{2C_{xy}C_{yx} - 2C_{xx}C_{yy}} & \frac{2C_{yy}K_{xy} - \mathrm{Cxy}(K_s + 2K_{yy})}{2C_{xy}C_{yx} - 2C_{xx}C_{yy}} & \frac{C_{yy}K_s}{2C_{xx}C_{yy} - 2C_{xy}C_{yx}} & \frac{C_{xy}K_s}{2C_{xy}C_{yx} - 2C_{xx}C_{yy}} & 0 & 0 \\
\frac{C_{yx}(K_s + 2K_{xx}) - 2C_{xx}K_{yx}}{2C_{xx}C_{yy} - 2C_{xy}C_{yx}} & \frac{C_{xx}K_s - 2C_{yx}K_{xy} + 2C_{xx}K_{yy}}{2C_{xy}C_{yx} - 2C_{xx}C_{yy}} & \frac{C_{yx}K_s}{2C_{xy}C_{yx} - 2C_{xx}C_{yy}} & \frac{C_{xx}K_s}{2C_{xx}C_{yy} - 2C_{xy}C_{yx}} & 0 & 0 \\
0 & 0 & 0 & 0 & 1 & 0 \\
0 & 0 & 0 & 0 & 0 & 1 \\
\frac{K_s}{M} & 0 & -\frac{K_s}{M} & 0 & 0 & 0 \\
0 & \frac{K_s}{M} & 0 & -\frac{K_s}{M} & 0 & 0
\end{pmatrix}
\tag{28}
$$

Having the Jacobian matrix of the system, we can write the system of coupled linear ODEs as

$$\dot{X} = \frac{\delta X}{\delta t} \cong f(X^n) + J(X)\delta X \tag{29}$$

The change in solution δX can now be found via solving a linear system such that

$$\left(\frac{I}{\delta t} - J(X)\right)\delta X = f(X^n) \tag{30}$$

where I, δX and $f(X^n)$ are $N \times 1$ matrices and $J(X)$ is a $N \times N$ matrix for a coupled system of N ordinary differential equations of first order. A direct solve of the linear system of equation (30) by Gaussian elimination will yield the change in solution δX from time-step n to $n+1$. The calculated change in solution can then be used as basis of first-order or second-order accurate implicit time integration schemes. The major benefit of implicit schemes is that their stability has minor to negligible sensitivity to chosen time steps and are therefore ideal for studying the dynamics of stiff dynamical systems as in the case of journal bearing supported shafts. As was explained above, a key step in implicit calculations is finding the Jacobian matrix at each time step which is inherently efficient if the Jacobian matrix can be found explicitly as in equation (28).

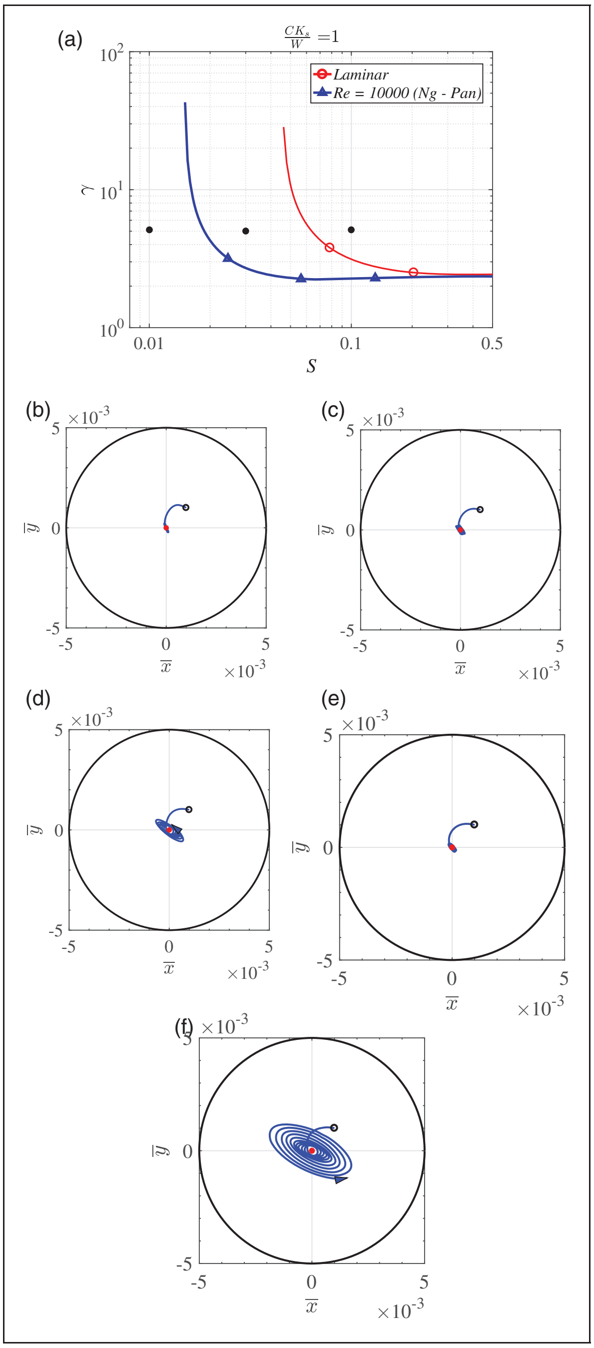

Figure 10. Journal bearing trajectory at three operating points (stars in (a)) under laminar (b, c and d) and turbulent (e, f and g) regimes of flow. (b) $S = 0.01$, $\gamma = 5$, (c) $S = 0.03$, $\gamma = 5$, (d) $S = 0.1$, $\gamma = 5$, (e) $S = 0.01$, $\gamma = 5$, (f) $S = 0.03$, $\gamma = 5$, (g) $S = 0.1$, $\gamma = 5$.

Non-dimensional journal trajectories in laminar and turbulent conditions, plot of $\bar{X}_{journal}$ *vs* $\bar{Y}_{journal}$ $\left(\bar{X} = \frac{X}{C}\right)$, at three different operating points were calculated by means of the detailed implicit time integration method of equations (25) to (30). The turbulent journal trajectory was based on the Ng–Pan–Elrod model at $Re = 10000$. The selected operating points (marked with bullets) and calculated trajectories are shown in Figure 10.

For all the cases shown in Figure 10, the journal center is released from a point very close to its steady-state point (within the radius of 0.1% of the journal clearance around the steady state point; marked with a hollow bullet) and its trajectory is followed in time. The first operating point is selected such that it lies in the stable region of both laminar and turbulent curves at $S = 0.01, \gamma = 5$. Similar results were obtained where journal finds its steady-state point, marked with a filled bullet, and remains there as shown in Figure 10(b) and (e). The next operating point $S = 0.03, \gamma = 5$ lies between the laminar and turbulent curves. As expected, the laminar-based trajectories, Figure 10(c), can still find the steady-state point while the turbulent-based trajectories, Figure 10(f), start to grow and hence becomes unstable. This again indicates that stable regions obtained based on the laminar theory can become unstable at higher Reynolds numbers. Both laminar and turbulent trajectories grow in the third selected operating point of $S = 0.1$, $\gamma = 5$ though with different speeds, Figure 10(d) and (g).

Conclusions and remarks

The stability bounds of a rotor-bearing system supported on turbulent journal bearings were presented in this study. Journal bearing coefficients are calculated based on the Reynolds equation that is modified for turbulent flows. Two turbulent models are used for stability analysis and the corresponding stability boundaries are compared. The predicted threshold speed of instability based on the Constantinescu's model was found to be higher than the threshold speeds predicted by the Ng–Pan–Elrod turbulent model and hence the latter model proves to be more conservative in design.

The stable region of flexible shafts supported on both turbulent and laminar journal bearings was shown to grow in size by increasing the shafts' non-dimensional parameter. It was found that at low load and high Sommerfeld region $S \geqslant 0.2$, the stability would not be affected by the type of flow within the bearing chamber and hence laminar analysis that is based on non-modified Reynolds equation is sufficient at these operating ranges. On the other hand, as the loading increases, the unstable operating region grows in size and will result in the unstable oil whirl to happen at even higher static loads, a region where the laminar-based stability analysis would be considered as a safe operating condition. Hence, modified stability analysis for turbulent flows needs to be implemented whenever the system is operating under high static load.

A numerical integration framework is presented in order to find the journal trajectories in the rotor-bearing system for laminar and turbulent flows. Results showed that the journal starts whirling at high Reynolds numbers in regions where the laminar stability criterion is considered as a "safe zone". This suggests that turbulent modifications are necessary for proper predictions of the system dynamics at high Reynolds numbers.

Declaration of Conflicting Interests

The author(s) declared no potential conflicts of interest with respect to the research, authorship, and/or publication of this article.

Funding

The author(s) disclosed receipt of the following financial support for the research, authorship, and/or publication of this article: The authors would like to thank the Qatar National Research Fund (QNRF) for partially funding this project.

References

1. Vance JM, Murphy B and Zeidan F. *Machinery vibration and rotordynamics*. Hoboken, NJ: John Wiley & Sons, 2010.
2. Vance JM. *Rotordynamics of turbomachinery*. New York, NY: John Wiley & Sons, 1988.
3. Lund J. Review of the concept of dynamic coefficients for fluid film journal bearings. *J Tribol* 1987; 109: 37–41.
4. Qiu Z and Tieu A. The effect of perturbation amplitudes on eight force coefficients of journal bearings. *Tribol Transact* 1996; 39: 469–475.
5. Choy FK, Braun MJ and Hu Y. Nonlinear effects in a plain journal bearing: Part 1—Analytical study. *J Tribol* 1991; 113: 555–561.
6. Andréas LS and De Santiago O. Identification of journal bearing force coefficients under high dynamic loading centered static operation. *Tribol Transact* 2005; 48: 9–17.
7. Meruane V and Pascual R. Identification of nonlinear dynamic coefficients in plain journal bearings. *Tribol Int* 2008; 41: 743–754.
8. Weimin W, Lihua Y, Tiejun W, et al. Nonlinear dynamic coefficients prediction of journal bearings using partial derivative method. *Proc IMechE, Part J: J Engineering Tribology* 2012; 226: 328–339.
9. Yang L-H, Wang W-M, Zhao S-Q, et al. A new nonlinear dynamic analysis method of rotor system supported by oil-film journal bearings. *Appl Math Model* 2014; 38: 5239–5255.
10. Hashimoto H and Wada S. An influence of inertia forces on stability of turbulent journal bearings. *Bull JSME* 1982; 25: 653–662.
11. Hashimoto H, Wada S and Ito J-I. An application of short bearing theory to dynamic characteristic problems of turbulent journal bearings. *J Tribol* 1987; 109: 307–314.
12. Wang J and Khonsari M. Application of Hopf bifurcation theory to rotor-bearing systems with consideration of turbulent effects. *Tribol Int* 2006; 39: 701–714.
13. Chang-Jian C-W and Chen CO-K. Bifurcation and chaos of a flexible rotor supported by turbulent journal bearings with non-linear suspension. *Proc IMechE, Part J: J Engineering Tribology* 2006; 220: 549–561.
14. Chang-Jian C-W and Chen C-K. Bifurcation and chaos analysis of a flexible rotor supported by turbulent long journal bearings. *Chaos Soliton Fractal* 2007; 34: 1160–1179.
15. Lund JW. *Self-excited stationary whirl orbits of a journal in a sleeve bearing*. PhD Thesis, Rensselaer Polytechnic Institute, 1996.
16. DiPrima R. A note on the stability of flow in loaded journal bearings. *ASLE Transact* 1963; 6: 249–253.
17. Taylor C and Dowson D. Turbulent lubrication theory—application to design. *J Lubricat Technol* 1974; 96: 36–46.
18. Constantinescu V. On turbulent lubrication. *Proc Inst Mech Eng* 1959; 173: 881–900.
19. Elrod H and Ng C. A theory for turbulent fluid films and its application to bearings. *J Lubricat Technol* 1967; 89: 346–362.
20. Adams ML. *Rotating machinery vibration: from analysis to troubleshooting*. Boca Raton, FL: CRC, 2009.
21. Szeri A Z. *Fluid film lubrication*. Cambridge, UK: Cambridge University Press, 2011.
22. Sawicki JT and Rao T. A nonlinear model for prediction of dynamic coefficients in a hydrodynamic journal bearing. *Int J Rotat Mach* 2004; 10: 507–513.
23. Gertzos K, Nikolakopoulos P and Papadopoulos C. CFD analysis of journal bearing hydrodynamic lubrication by Bingham lubricant. *Tribol Int* 2008; 41: 1190–1204.
24. Miraskari M, Hemmati F, Jalali A, et al. A robust modification to the universal cavitation algorithm in journal bearings. *J Tribol* 2016.
25. Celik IB, Ghia U and Roache PJ. Procedure for estimation and reporting of uncertainty due to discretization in CFD applications. *J Fluid Eng Transact ASME* 2008; 130.
26. Raimondi AA and Szeri AZ. CRC Handbook of Lubrication (Theory and Practice of Tribology) In: Booser ER (ed.) *Journal and Thrust Bearings*, 1984, pp. 413–462.

Appendix

Notation

C	radial clearance (m)
C_{ij}, $\bar{C}_{ij}$	damping coefficients in Cartesian coordinates $i, j = x, y$ and in (R-T)

	coordinates $i,\ j = R,\ T$ where $\bar{C}_{ij} = \frac{C\,\omega}{L\,D\,\mu\,N\left(\frac{R}{C}\right)^2}\ C_{ij}$
$[\bar{C}]_{x-y}$, $[\bar{C}]_{R-T}$	non-dimensional damping matrix in x-y and R-T coordinate systems
e	eccentricity, m
$\%e_a^{21}$, $\%e_{ext}^{21}$	fine grid approximate and extrapolated relative errors in numerical calculation of the field variable
$F_x,\ F_y,\ F_R,\ F_T$	total bearing reaction forces in $x,\ y,\ R,\ T$ directions, N
$f_x,\ f_y$	bearing dynamic reaction force in excess of bearing steady state force in x and y directions, N
$f(\boldsymbol{X}, t)$	right hand side of the state space equations of motion
GCI_{fine}^{21}	the fine grid convergence index
h	oil film thickness, $h = C(1 + \epsilon\cos(\theta))$, m
$J(\boldsymbol{X})$	Jacobian matrix of the coupled system of ODEs of the dynamical system
$K_{ij},\ \bar{K}_{ij}$	stiffness coefficients in Cartesian coordinates $i,\ j\ =\ x, y$ and in (R-T) coordinates $i,\ j = R,\ T$ where $\bar{K}_{ij} = \frac{C}{L\,D\,\mu\,N\left(\frac{R}{C}\right)^2}\ K_{ij}$
$K_s,\ \bar{K}_s$	shaft stiffness where $\bar{K}_s = \frac{C}{L\,D\,\mu\,N\left(\frac{R}{C}\right)^2} K_s = \frac{1}{S}\frac{C\,K_s}{W}$
$k_\theta,\ k_z$	circumferential and longitudinal turbulent coefficients
L	journal bearing Length
M	reduced mass of the rotor
γ	stability parameter: $\gamma = \frac{C\,K_s}{W}\bar{\omega}_{th}^2$
N	rotating speed, $\frac{rev}{sec}$
$O_J,\ O_M$	geometric center of the journal and the central disc
$P,\ \bar{P}$	unsteady pressure: $\mathrm{P} = \frac{\mathrm{P}}{\mu\,N\left(\frac{R}{C}\right)^2}$
$P_0,\ P_R,\ P_T,\ P_{\dot{R}},\ P_{\dot{T}}$	steady pressure and its gradients in R-T coordinates
Q	rotation matrix
R	journal radius, m
Re	average Reynolds number: $Re = \frac{\rho\,R\,\omega\,C}{\mu}$
Re^*	local Reynolds number: $Re^* = \frac{\rho\,R\,\omega\,h}{\mu}$
S	Sommerfeld number: $S = \frac{L\,D\,\mu\,N}{W}\left(\frac{R}{C}\right)^2$
t	time (s)
W	load per bearing ($\frac{Mg}{2}$)
$x,\ y,\ R,\ T$	Cartesian and rotated coordinate systems. The R coordinate is aligned with the line of centers.
$\dot{x}, \dot{y},\ \dot{R},\ \dot{T}$	velocity components in Cartesian and rotated coordinate systems
X_i	state–space variables of the dynamical system. $i\ =\ 1, 2, \ldots, 6$
$\boldsymbol{X}^n,\ \boldsymbol{X}^{n+1}$	state–space vector at time-step n and $n{+}1$
$\delta\boldsymbol{X}$	change in solution of the dynamical system from two consecutive time-steps
$\bar{X}_{journal}$, $\bar{Y}_{journal}$	dimensionless journal center displacement in horizontal and vertical directions
γ	stability parameter: $\gamma = \frac{C\,K_s}{W}\bar{\omega}_{th}^2$,
ϵ	eccentricity ratio $\epsilon = \frac{e}{C}$
θ	circumferential coordinate
θ_{cav}	the cavitation boundary
μ	fluid film (lubricant) viscosity (Pa.s)
$\nu,\ \bar{\nu}$	whirl frequency $\nu = \omega\bar{\nu}$
ρ	fluid film density (kg/m^3)
φ	attitude angle
Φ_{ext}^{21}	extrapolated field variable in fine grid
$\Phi_1, \Phi_2,\ \Phi_3$	numerical estimate of the field variable in fine, medium and coarse mesh
ω	shaft rotating speed (rad/s)
$\bar{\omega}$	dimensionless shaft rotating speed ($\omega\sqrt{M/K_s}$)
$\bar{\omega}_{th}$	dimensionless threshold speed of instability